Title

Comparison of Klinkenberg-corrected gas permeability and water permeability in sedimentary rocks

Authors

Wataru Tanikawa[1]*

Toshihiko Shimamoto[2]

Addresses

1. Kochi Institute for Core Sample Research, Japan Agency for Marine-Earth Science and Technology (JAMSTEC), 200 Monobe-otsu, Kochi, Japan.
2. Department of Earth and Planetary Systems Science, Graduate School of Science, Hiroshima University, Higashi-Hiroshima, Japan

*Corresponding author

Address: Kochi Institute for Core Sample Research, Japan Agency for Marine-Earth Science and Technology, Nankoku 783-8502, Japan

Tel: +81-88-878-2203; fax: +81-88-878-2192

E-mail: tanikawa@jamstec.go.jp

Abstract

Quick measurements of permeability can be made by using gas as the pore fluid. To apply gas permeability data to the evaluation of water permeability, the difference between gas and water permeabilities needs to be assessed. We measured intrinsic permeability of sedimentary rocks from the western foothills of Taiwan by using nitrogen gas and distilled water as pore fluids in effective-pressure cycling tests at room temperature. The observed difference in gas and water permeabilities was analyzed in view of the Klinkenberg effect. This effect is due to the slip flow of gases at pore walls, which enhances gas flow when pore sizes are very small. Our experimental results showed that (1) gas permeability was larger than water permeability by several times to one order of magnitude, (2) gas permeability increased with increasing pore pressure, and (3) water permeability increased slightly as the pore-pressure gradient across the specimen increased. Results (1) and (2) can be explained quantitatively by an empirical power law in relation to the Klinkenberg constant b that is applicable in low permeable range. This correlation enables us to estimate water permeability from gas permeability. The Klinkenberg effect is important when permeability is lower than 10^{-18} m^2 and at low pore-pressure differentials, and correction for the effect is essential to estimate water permeability from gas permeability measurement data. A simplified Bingham flow

model for water can partially explain the trend of result (3), though non-Darcy flow behavior or inertial forces of water-rock interaction are needed to account for the observed deviation from Darcy's law.

Keyward

Gas permeability; Water permeability; Klinkenberg effect; Sedimentary rock

1. Introduction

Permeability (or intrinsic permeability) is an important controlling parameter of fluid flow systems at depth. Permeability ranges widely from more than 10^{-12} to less than 10^{-23} m^2 depending on the rock type and depth [1, 2]. Permeability measurements under high confining pressure in a laboratory are one possible way to predict permeability structure at depth. One of the simplest methods to measure permeability is the steady-state method. Moreover, the use of gas as a pore fluid instead of water for the permeability measurement has the following advantages: (1) commercial gas flow-meters that cover a wide range of flow rates for all gases are available, allowing the measurement of a wide range of permeabilities quickly and accurately; (2) nitrogen gas is chemically inert, allowing geochemical effects to be ignored, so only permeability variation caused by change in confining pressure need be considered; and (3) the compressibility and viscosity of gas are less sensitive to temperature changes than those of water, so permeability measurement error due to these factors is less likely to be introduced.

Ideally, permeability does not depend on the type of pore fluid; therefore, permeability measured by using gas should be the same as that measured by using water. Several fluid-flow problems have been analyzed using permeabilities measured by

using gas instead of water [3-5]. However, it has been found that (1) permeability of a medium to gas changes in relation to pore-pressure changes at the same effective pressure [6], and (2) permeability of a medium to gas is higher than the permeability of the same medium to water [7]. These problems might be related to the pore-pressure dependence of gas permeability known as the Klinkenberg effect [8], which we define and discuss in detail in Section 2. There are few examples, however, in which permeabilities to different pore fluids are compared in the same samples [7,9-10] under high confining pressure. Therefore, in this study, permeability of the same specimens measured by using nitrogen gas as the pore fluid was compared with that measured by using water as the fluid in effective-pressure cycling tests. Then, the Klinkenberg effect on gas permeability and the pore-pressure dependence of permeability are discussed in relation to the experimental data. Furthermore, the relationship between the Klinkenberg slip factor and water permeability in low permeability range is discussed as the relationship in low permeable rocks is not well studied. Sedimentary rocks from the western foothills of Taiwan that have permeability variations were used for the permeability measurements.

2. Intrinsic permeability and the Klinkenberg effect

Intrinsic permeability is a measure of the mobility of fluid within a porous material that is related solely to the pore geometry of the rock (porosity, pore shape, pore-size distribution, etc.), and it is independent of the properties of the fluid. Therefore, intrinsic permeability measured by using any gas as the pore fluid in a laboratory test should be the same as that measured by using any other kind of fluid. Hydraulic conductivity is a function of both the medium and the properties of the fluid, and its relationship to intrinsic permeability is given by

$$K = \frac{k}{\eta}\rho g \quad , \tag{1}$$

where K is hydraulic conductivity (m/s), k is intrinsic permeability (m^2), η is the viscosity of the fluid (Pa·s), ρ is the fluid density (kg/m^3), and g is gravitational acceleration (m/s^2). Equation (1) indicates that fluid mobility depends on fluid viscosity, density and gravity. Klinkenberg [8] discovered that the permeability of a medium to gas is relatively higher than that as water, and he interpreted this phenomenon to "slip flow" between gas molecules and solid walls. In Darcy flow, molecular collisions dominate and collisions between the gas molecules and the pore wall, which are described as adherence at the fluid–solid boundary, are neglected. As the pore radius approaches the mean free path of the gas molecules, the frequency of collisions between gas molecules and the solid walls increases. Therefore, this additional flux due to gas flow at the wall surface, which is called "slip flow," begins to effectively enhance the

flow rate. This phenomenon is called the *Klinkenberg effect* and is expressed as follows:

$$k_g = k_l\left(1+\frac{4cl}{r}\right) = k_l\left(1+\frac{c\kappa}{\pi\sqrt{2}r^3}\frac{T}{P}\right) = k_l\left(1+\frac{b}{P}\right), \quad b = \frac{c\kappa T}{\sqrt{2}\pi r^3} \tag{2}$$

where k_g is the permeability of a medium to gas (m^2), k_l is the permeability of a medium to liquid (m^2), l is the mean free path of the gas molecules (m), r is the pore radius (m), κ is Boltzmann's constant (JK^{-1}), T is temperature (K), c is a constant, P is pore pressure (Pa), and b is the Klinkenberg slip factor (Pa). The value of the parameter l in equation (2) is given by the following relationship [11]:

$$l = \frac{\kappa}{4\pi\sqrt{2}r^2}\frac{T}{P} \tag{3}$$

Equation (2) indicates that if the pore radius and the gas pore pressure are small and the temperature of the gas is high, then k_g becomes much larger than k_l; in contrast, k_g approaches k_l as pore pressure approaches infinity. For this reason, Brace et al. [9] and Zoback and Byerlee [12] performed gas permeability tests under high pore pressure conditions (P = 5 to 15 MPa) by the transient flow method to avoid the Klinkenberg effect. Brace et al. (1968) showed that the permeability of Westerly granite to water, ranging from 10^{-16} to 10^{-18}, was similar to that as argon gas; however, it was not mentioned that how high a pore pressure was required to avoid the Klinkenberg effect

118 in gas permeability tests.

119 The Klinkenberg factor b depends on the rock properties, and to a lesser degree on
120 the physical properties of the gas. Previous researches showed that b took a wide range
121 of values from 10^{-2} [8] to 18 [6]. Jones [13] investigated the relationship between the
122 Klinkenberg slip factor b and estimated water permeability k_l in about 100 core
123 samples, and found that log b increased linearly with log k_l within a permeability range
124 from 10^{-12} to 10^{-17} m^2. Persoff and Hulen [14] estimated the relationship between b and
125 k_l in less permeable (10^{-18} to 10^{-22} m^2) metagraywacke samples; their results were
126 generally consistent with those of Jones, except that the slope of the regression line
127 was apparently steeper than that obtained by Jones [13], although they used too few
128 data points (8 points) to be sure.

129

130 **3. Sample information and method**

131

132 Outcropping sandstones from the west-central part of the western foothills of Taiwan
133 (Pleistocene to Miocene rocks) were used for our permeability tests. The western
134 foothills are known to be in a fold and thrust belt that developed during the Miocene as
135 a result of the collision of the Luzon arc with the Asian continent [15]. The western
136 foothills are well known for oil and natural gas fields [16], and permeability at depth in

137 the western foothills is a key parameter for understanding oil and natural gas storage
138 and migration mechanisms.
139 All samples were cored to a cylindrical shape. All specimens were 5 to 40 mm long and
140 approximately 20 mm in diameter. 4 samples were used for the comparison between gas
141 and water permeabilites, and gas permeability were measured in 30 samples to show the
142 relationship between *b* and permeability. Specimens were dried at 80 °C in an oven to
143 eliminate pore water before the gas permeability measurement. All experiments were
144 performed at room temperature using the intravessel oil pressure apparatus at Kyoto
145 University. In this experimental system, the oil apparatus can attain a confining pressure
146 of up to 400 MPa in conjunction with a mini-pressure generator system. To confine the
147 pressure, avoid leakage, and eliminate bypass flow between the side of the sample and
148 the jacket during permeability tests, samples were jacketed in three to four layers of
149 polyolefin, which contracts during heating. Fluid flows from the bottom to the top of a
150 specimen in this apparatus.
151 When an incompressible fluid (liquid) is used for permeability tests, intrinsic
152 permeability *k* is determined from the linear form of Darcy's law:
153 $$Q = -\frac{kA}{\eta}\frac{dP}{dx},$$
154 (4)
155 where Q is the volume of fluid measured per unit time, A is the cross-sectional area of

156 the sample, η is viscosity of the pore fluid, and *dP/dx* is the pressure gradient.
157 One-dimensional gas flow is assumed in equation (4) as the enforced pressure gradient
158 during permeability tests is very large. If a constant pressure gradient through the
159 sample is assumed, then equation (4) can be expressed as
160
161 $$Q = \frac{kA}{\eta L}\left(P_{up} - P_{down}\right)$$
162 (5)

163 L is sample length and P_{up} and P_{down} are pore pressure at the upstream end (x = 0) and
164 downstream end ($x = L$) of the specimen, respectively. However, when a compressible
165 gas (PV = constant) is used as the pore fluid, the density of the pore fluid differs within
166 the specimen. In this case, the average gas permeability k_{gas} is expressed as [6]

167 $$Q(x) = \frac{Ak_{gas}}{\eta}\frac{\frac{1}{2}\left(\frac{P_{up}{}^2 - P_{down}{}^2}{L}\right)}{\sqrt{P_{up}{}^2 - \frac{P_{up}{}^2 - P_{down}{}^2}{L}x}}$$
168 (6)

169 . When $x = L$, equation (6) becomes

170 $$Q(x = L) = \frac{Ak_{gas}}{2\eta L}\left(\frac{P_{up}{}^2 - P_{down}{}^2}{P_{down}}\right)$$
171 (7) [17].

172 In our apparatus, P_{up} was kept constant at a value between 0.2 and 2 MPa using the

173 gas regulator, and the gas flow rate was monitored at the downstream of the samples
174 (Figure 1). Fluid flowing out of the specimen at the downstream end was released to
175 atmospheric pressure, and P_{down} was assumed to have a constant value of 0.1 MPa. Thus,
176 the pore-pressure differential, $P_{up} - P_{down}$, can be assumed to be constant, and equation
177 (7) can be applied to evaluate gas permeability. The volumetric gas flow rate at the
178 downstream end of the samples was measured with a digital gas flow-meter
179 (ADM2000; Agilent Technologies, USA) and a high-precision bubble gas flow meter
180 (VP-1U; HoribaSTEC Ltd, JAPAN). Continuous, real-time digital measurements are
181 made by the ADM2000, enabling fast measurement of the gas permeability. Several
182 seconds to more than 10 minutes can be required to measure a volumetric flow rate with
183 the VP-1U, though a very low flow rate can be achieved. The ADM2000 can measure a
184 volumetric flow rate within the range 0.0005 –1.0 L/min (accuracy, ±3% of reading, or
185 ±0.2 mL/min, whichever is greater), and the VP-1U can measure a flow rate within the
186 range 0.024–10 mL/min (accuracy, ±0.5% for 0.2–2 mL/min; ±1% for 2–10 mL/min).
187 Therefore, a wide range of gas flow rates from 1 L/min to 0.024 mL/min, corresponding
188 to gas permeabilities from 10^{-13} m^2 down to 10^{-19} m^2 in our experiments, was easily
189 measured by using these gas flow-meters.

190 Water permeability was evaluated by the steady-state flow method, by using
191 equation (5). Upstream pore pressure was controlled in the same way as before.

192 Distilled water was stored in the water tank and directly pressurized by nitrogen gas
193 from the gas bottle. Pore water at the downstream end was released to atmospheric
194 pressure. The water flow rate at the downstream end was determined by using a digital
195 balance (GF400; A&D Company, Ltd., JAPAN) to continuously monitor the real-time
196 weight increment of water flowing out from the specimen. Therefore, there was no
197 lower limit for the water permeability measurement if time permitted. We observed no
198 gas bubbles in the water flowing out from the downstream line during the water
199 permeability measurements, indicating that two-phase (water and nitrogen gas) flow did
200 not occur, even though we forced the water from the water tank with nitrogen gas under
201 high pressure. The viscosities of the nitrogen gas and distilled water at room
202 temperature of 17.4×10^{-6} Pa・s and 1.0×10^{-3} Pa・s were used for the permeability
203 evaluation.

204 Permeability was measured at confining pressures that stepped up from 5 MPa to
205 the maximum of 160 MPa. To compare permeability of a medium to nitrogen gas with
206 that of same medium to water, nitrogen gas was used as the pore fluid for the first and
207 second, or first, second, and third, pressure cycles, and then distilled water was used as
208 the pore fluid for the last two pressure cycles. Before the pore fluid was switched from
209 nitrogen gas to water, the pore flow line was vacuumed once for an hour, and then filled
210 with CO_2. After we vacuumed for an hour again, distilled water was poured into the

211 specimens. By filling the pore flow lines once with CO_2, we could minimize the
212 influence of gas remaining within the pores during the water permeability measurement,
213 because the solubility of CO_2 in water is quite large under high pressure so that any CO_2
214 gas would dissolve in the water during tests. The pore-pressure dependence of
215 permeability was investigated by changing P_{up} while keeping the confining pressure
216 constant.
217
218 **4. Experimental result**
219
220 General information on the test samples used to compare the difference between water
221 and gas permeability is given in Table 1. Porosity was measured by the standard method,
222 where porosity is calculated from the weight difference between the water-saturated
223 sample and the dry sample, and by the mercury intrusion porosimetry technique (MIPT)
224 with a commercial porosimeter (Porosimeter 2000, Carlo Erba Ltd.). The MIPT yielded
225 lower porosity than that determined by the standard method. Pore-size distributions
226 were also measured by MIPT (Figure 1). The radius of most micropores was in the
227 range from 0.01 to 10 μm. The peak volumetric ratio was near the maximum end of the
228 pore-size range in each case. Sample IVA407 (Tungkeng Fm), which had the highest
229 porosity among the specimens, also had the largest average and modal pore radii.

230 The results of the pressure cycling tests on the sandstone specimens are shown in
231 Figure 2. Permeability was plotted against the effective pressure, defined as the
232 difference between the confining pressure and the pore pressure. In our tests, however,
233 the effective pressure was assumed to be equivalent to the confining pressure because
234 the pore pressure was extremely small compared with the confining pressure. The error
235 bars in the figure mainly reflect differences caused by pore-pressure variation, because
236 permeability varies significantly with changes in pore pressure (this pore-pressure
237 dependence of permeability is described in the following section). The accuracy of the
238 flow rate was less than 1%, and the error of each data point is within the symbol.
239 In sample IVA407, five effective-pressure cycles were conducted. During the first
240 three pressure cycles, nitrogen gas was used as the pore fluid, and distilled water was
241 used during the other two pressure cycles. The initial permeability at the lowest
242 effective pressure was around 10^{-13} m^2, and permeability decreased as the effective
243 pressure increased, although permeability was reduced by less than one order of
244 magnitude from the initial value even at 100 MPa of effective pressure. The
245 permeability during the first cycle was relatively larger than that during the second or
246 third pressure cycles, and a similar cyclic path was described during the second and
247 third cycles. Soon after the pore fluid was changed from nitrogen gas to water, the
248 permeability decreased sharply; the permeability of the medium to nitrogen gas was 2 to

4 times that of the same medium to water at the same effective and differential pressures. Permeability during the fifth cycle was relatively smaller than that during the fourth cycle. The influence of the pore fluid on the permeability change was larger than that caused by the change in effective pressure or the increase in the pressure cycle number (shown by error bars) for the same fluid. The other specimens (IVA418, IVA419, and IVA478) showed similar permeability behavior as the pressure cycle tests with IVA407, although the difference between the gas and water permeability differed among specimens. In the case of IVA419, with smaller permeability than IVA407, permeability to gas was 5 to 7 times that to water. In IVA418 and IVA478, which had the lowest permeabilities, permeability of a medium to gas was more than 10 times that of the same medium to water. These results imply that the permeability difference between nitrogen gas and water is larger in specimens with low intrinsic permeability. The permeability was also correlated with porosity and pore-size distribution; in our test samples, permeability of porous sandstones with larger pore size (IVA407, IVA419) was higher than that of the less porous sandstones (IVA418, IVA478). In IVA418, a sudden irregular drop of permeability was recognized at 40 MPa during the third cycle, but this drop was not observed during the other cycles or in other specimens. Wetting may enhance deformation by mechanical collapse, because it is generally true that rocks are weaker when wet than when dry. Therefore, an unexpected mechanical collapse might

have occurred at the time of wetting, but we do not have direct evidence of this from microstructural observations.

Figure 3 illustrates examples of the relationship between the permeability to nitrogen gas and the pore-pressure differential. Generally, permeability decreases as the pore-pressure differential increases at all effective pressures. In IVA419, the maximum permeability differed by a factor of 1.6 for pore-pressure differentials between 0.2 and 0.8 MPa.

The relationship between the permeability to water and the pore-pressure differential is shown in Figure 4. In IVA419, permeability increased as the pore-pressure differential increased, a trend opposite to that for permeability to gas. The maximum permeability differed by a factor of 1.5 in relation to pore-pressure differential changes. In IVA478, however, a dependence of permeability on the pore-pressure differential was not clear.

5. Discussion

5-1. Klinkenberg effect

We plotted the permeability to nitrogen gas against the inverse of the average pore

287 pressure, $1/P_{av}$, ($P_{av} = (P_{up}+P_{down})/2$) to verify the Klinkenberg effect (Figure 5). In most
288 cases, the permeability to gas increased linearly as $1/P_{av}$ increased, a result that is
289 consistent with the Klinkenberg equation, if it is assumed that average pore pressure is
290 equivalent to the pore pressure P in equation (2). Therefore, the permeability to water k_l
291 can be estimated from the slopes of the lines in Figure 6. Water permeability estimated
292 by using the Klinkenberg equation, equation (2), showed almost the same value as the
293 observed permeability to water in IVA478, but in IVA407, IVA418, and IVA419, the
294 estimated water permeability was smaller than the observed permeability, though except
295 in IVA407 the difference was much smaller than the difference between water and gas
296 permeabilities (Figure 6). These results suggest that the difference between gas and
297 water permeabilities is strongly affected by the Klinkenberg effect. In IVA407, the
298 estimated water permeability did not show a linear relationship with average pore
299 pressure.

300 The pressure dependence of nitrogen gas viscosity can also cause a pore-pressure
301 dependence of permeability to gas. Nitrogen gas viscosity exhibits a positive
302 dependence on pressure, which can increase the permeability to gas, though this
303 sensitivity is much smaller than the temperature dependence. However, in our
304 experiment, the permeability change due to differences in pore pressure is so large that
305 the small pressure dependence of nitrogen gas viscosity (17.87 μPa·s for 0.1 MPa and

306 17.94 for 2 MPa at 300 K; [18]) cannot explain the observed pore pressure dependence
307 of permeability to gas.
308
309 **5-2. Klinkenberg slip factor**
310
311 Not only the water permeability but also the Klinkenberg slip factor *b* can be
312 approximated from the fitted slopes (Figure 5). When parameter *b* was plotted against
313 water permeability, both estimated from equation (2), for 30 sedimentary rocks from the
314 western foothills (330 points) (Figure 7), we found that *b* decreased with increasing
315 permeability to water, although the data show considerable scatter. The relationship
316 between water permeability and parameter *b* is described by the formula
317 $$b = (0.15 \pm 0.06) \times k_l^{(-0.37 \pm 0.038)}, \quad (8)$$
318 when the units of k_l and *b* are selected as m^2 and Pa, respectively. This correlation was
319 previously studied by Heid et al. [19], Jones [13], and Jones and Owens [20] for
320 different permeability ranges. Heid et al. [19] showed the correlation in air at 25 °C as
321 $$b = 0.11 k_l^{-0.39} \quad (9)$$
322
323 for oil-field cores with permeability values of about 10^{-12} and 10^{-17} m^2. Jones and
324 Owens [20] measured permeabilities of between 10^{-14} and 10^{-19} m^2 for low-permeable

sands, and the correlation with b was expressed as

$$b = k_l^{-0.33}. \quad (10)$$

Both correlations are quite similar to our results, though in our tests the b values were slightly smaller for all permeability ranges. Moreover, for permeabilities less than 10^{-19} m^2, the slope of the relationship seems to become steeper, a trend also shown by Persoff and Hulen [14].

When the correlation described by equation (8) is assumed to be applicable to any rocks, and when equation (8) substitutes into equation (2), the relationship between permeability to gas and that to water is

$$k_g = k_l\left(1 + \frac{0.15k_l^{-0.37}}{P_{av}}\right). \quad (11)$$

Therefore, the relationship between the ratio of permeability to gas and permeability to water, k_g/k_l, and the pore-pressure differential, $P_{up} - P_{down}$, in our experimental settings that P_{down} = 0.1 MPa (Figure 8) is such that when permeability of a medium to water is higher than 10^{-16} m^2, k_g/k_l is less than 2 for all values of the pore-pressure differential. However, when permeability of a medium to water is less than 10^{-17} m^2, the discrepancy between k_g/k_l values for different values of the pore-pressure differential becomes

larger: in the extreme case, k_g/k_l is 30 when k_l is 10^{-20} m^2 and the pore-pressure differential is 0.05 MPa. Therefore, we cannot neglect the difference between gas and water permeability when both permeability and the pore-pressure differential applied for the permeability measurements are smaller than 10^{-17} m^2 and 0.2 MPa respectively.

5-3. Pore-pressure dependence of water permeability

Several specimens showed a dependence of permeability of a medium to water on the pore-pressure differential (Figure 4). Sasaki et al. [21] suggested that this positive dependence is caused by Bingham plastic flow within small pores. Byerlee [22] also asserted that fluid that flows within a relatively impermeable fault zone may exhibit Bingham flow, which may increase the fluid pressure in the fault zone, thus reducing fault strength. Generally, water exhibits Newtonian flow, in which the permeability does not depend on the pore-pressure differential. However, when pore spaces are small, adhesion to pore walls causes resistance to water flow, leading to a smaller flow rate and smaller permeability. The Buckingham-Reiner equation describing Bingham flow in a one-capillary-tube model is [23]

$$Q = \frac{\pi \Delta P R^4}{8 L \eta_p}\left[1 - \frac{4}{3}\left(\frac{2L\tau_o}{R\Delta P}\right) + \frac{1}{3}\left(\frac{2L\tau_o}{R\Delta P}\right)^4\right],$$

(12)

where Q is the volumetric flow discharge, ΔP is the pressure difference, R is the radius of the capillary tube, η_p is the slope of the relationship between shear stress and the rate of shear or dynamic viscosity when the shear stress $\tau > \tau_0$, L is the length of the tube, and τ_0 is the critical yield strength. Under Newtonian flow, τ_0 becomes 0 and equation (12) becomes the Hagen-Poiseuille law:

$$Q = \frac{\pi \Delta P R^4}{8 L \eta_p}. \tag{13}$$

If we apply the Buckingham-Reiner equation to porous media, assuming that a capillary tube is analogous to a pore with radius $r = R$, permeability to a Bingham plastic fluid can be expressed by combining Darcy's law (equation 4) with equation (12):

$$k_l = \frac{Q \eta_w L}{A \Delta P} = \frac{n r^2}{8}\left[1 - \frac{4}{3}\left(\frac{2L\tau_o}{r\Delta P}\right) + \frac{1}{3}\left(\frac{2L\tau_o}{r\Delta P}\right)^4\right], \tag{14}$$

where n is porosity , η_w is the viscosity of water, and $\eta_p = \eta_w$ is assumed, and the relationship between porosity of the medium, n, and pore radius ($\pi r^2 = nA$) that contains, on average, one capillary for a cross-sectional area A is applied. This correlation can be employed if it is assumed that pore size can be represented by a single pore size, implying that water permeability reaches the stable value $nR^2/8$ at

379 larger pressure differentials. Two examples of the dependence of permeability on the
380 pore-pressure differential are shown in Figure 10. The experimental result for IVA389
381 (the same specimen as IVA418 but a different experimental run) of 30 MPa of effective
382 pressure was compared to the result calculated using equation (14), which assumes that
383 all pores are the same size. Parameters τ_0 and R were evaluated by the least-squares
384 method as 0.25 MPa and 0.13 μm, respectively. The prediction curve reaches a
385 permeability of $2.9 \cdot \times 10^{-16}$ m^2 at a higher pressure differential. This curve is partly
386 consistent with our experimental data, showing that permeability increases as the
387 pore-pressure differential increases and that the pressure sensitivity decreases gradually
388 as the pressure differential increases, but it does not reproduce them perfectly. The result
389 for IVA478 shows similar behavior.

390 As shown by the pore-size distribution of IVA418 (Figure 1), the pore radius of the
391 test specimens ranged widely from 0.01 to 10 μm, and the modal pore size was several
392 times larger than the pore size approximated by using equation (14). The discrepancy
393 between the two might be caused by the application of a simplified equation that
394 assumes that the pore size of a sample can be characterized by a single representative
395 pore size. When the pore-size distribution is taken into account, which is the more
396 realistic case, equation (14) is rewritten as

397 $$k_l = \sum k_i f(r_i) = n \sum f(r_i) \frac{r_i^2}{8} \left[1 - \frac{4}{3} \left(\frac{2L\tau_{io}}{r_i \Delta P} \right) + \frac{1}{3} \left(\frac{2L\tau_{io}}{r_i \Delta P} \right)^4 \right], \quad (15)$$

398 where $f(r_i)$ is the volumetric ratio of a pore of radius r_i. It is also realistic that τ_{i0} is
399 related to pore geometry and can change with pore radius. Equation (15) assumes that
400 the radius of each pore does not change in the flow direction through the specimen. The
401 other simplification is that the pore structure is partitioned into several parts
402 perpendicular to the flow direction. In this case, the equivalent permeability is given by
403 the harmonic mean of the individual permeabilities,

404 $$k_l = \frac{1}{\sum \frac{f(r_i)}{k_i}} . \quad (16)$$

405

406 Using the pore-size distribution measured by the MIPT, permeability can be evaluated
407 by these capillary tube models. The gas and water permeabilities determined by
408 laboratory experiment were compared to the results of the three capillary models
409 described by equations (14), (15), and (16) (Figure 10). Permeabilities calculated
410 assuming an effective pressure of 10 MPa were plotted against the experimental values.
411 The average pore radius (Table 1) was used in equation (14), and the pore-size
412 distributions shown in Figure 2 were used in equations (15) and (16). To avoid the
413 unknown parameters, τ_0 = 0 was selected. The data suggest that permeability is
414 influenced by the average pore radius, though the estimated values are large for all

415 specimens. The experimental values are between the harmonic and arithmetic means of
416 the capillary model. The simplest model, equation (14), is the most suitable for
417 estimating gas permeability, and the harmonic mean model yields more reasonable
418 results in low permeability specimens. Therefore, it can be said that permeability of
419 relatively porous rocks is controlled by the larger pore sizes (arithmetic mean model
420 domination), whereas the permeability of impermeable samples is more influenced by
421 the smaller pores (harmonic mean model domination).

422 It is not clear whether the chosen value of τ_0 is realistic in nature. Furthermore,
423 several data points do not show clearly the dependence of the water permeability on the
424 pore-pressure differential. Even though the positive pore-pressure dependence in our
425 water permeability test can be partially explained by the Buckingham-Reiner equation,
426 water interactions with clays or inertial effects [24, 25] and the non-Darcy flow that is
427 described as the Forchheimer equation [26] must have considered explaining our data
428 thoroughly.

429 Our laboratory experiments were focused on porous sedimentary rocks, though it is
430 unknown whether other rocks (incohesive rocks, granite, fractured rocks, etc.) would
431 exhibit the same permeability characteristics. Faulkner and Rutter [7] compared the
432 permeability of clay-rich fault rocks to argon and water. Their data suggest that
433 permeability of a medium to argon gas was 10 times that of the same medium to water,

434 which in general is consistent with our results. However, they concluded that the
435 difference was caused by a reduction of the effective pore diameter due to the adhesion
436 of water molecules to crystal surfaces rather than to the Klinkenberg effect or Bingham
437 plastic flow behavior. It is possible that several mechanisms might concurrently affect
438 water and gas flow and permeability to each in a specimen. Therefore, understanding
439 the dominant mechanism accounting for permeability differences under various
440 conditions in relation to specimen characteristics such as pore shape and mineral
441 composition is important for our future study.
442
443 **6. Conclusions**
444
445 The permeability of sandstone specimens from the Taiwan western foothills to nitrogen
446 gas and water was measured on the same specimens in effective pressure cycling tests,
447 yielding the following significant results. (1) The permeability of a given specimen to
448 nitrogen gas was 2 to 10 times that to water. (2) The permeability to nitrogen gas
449 decreased as pore pressure increased, and this pore-pressure dependence on the
450 permeability of a medium to gas could be explained by the Klinkenberg equation for
451 most experimental data. The water permeability estimated by using the Klinkenberg
452 equation was consistent with the observed water permeability. (3) The relationship

453 between the Klinkenberg slip factor *b* and water permeability was consistent with that
454 determined empirically by a previous study, namely, that log *b* decreases linearly as log
455 water permeability increases over a wide range from 10^{-14} to 10^{-20} m^2. (4) The
456 permeability to water was positively related to the pore-pressure differential and
457 pore-size distribution, which can be partially explained by the Buckingham-Reiner
458 equation, though the calculated curve does not fully reproduce the experimental data
459 because of the complex pore geometry of the specimens, inertial effects nor non-Darcy
460 flow behavior that are .

461 Our experimental results suggest that the difference between the permeability of a
462 medium to gas and that of the same medium to water can be partly explained by the
463 Klinkenberg effect. Therefore, gas permeability values should not be corrected by using
464 the Klinkenberg equation when the Klinkenberg effect is not relevant. This phenomena
465 is only significant for low permeability media. The pore-pressure dependence of both
466 water and gas permeabilities should also be taken into account in fluid flow problems.

467

468

469 **Acknowledgements**

470

471 We express special appreciation to Dr. Weiren Lin of the Japan Agency for

Marine-Earth Science and Technology (JAMSTEC), and Mr. Daisaku Satou and Dr. Manabu Takahashi of the National Institute of Advanced Industrial Science and Technology (AIST) of Japan for the data on pore-size distributions obtained by mercury injection tests.

References

[1] Neuzil CE. How permeable are clays and shales? Water Resources Res 1994;30: 2:145-150.

[2] Wang HF. Theory of linear poroelasticity: with applications to geomechanics and hydrogeology. Princeton: Princeton University Press, 2000.

[3] Wibberley C. Hydraulic diffusivity of fault gouge zones and implications for thermal pressurization during seismic slip. Earth Planets and Space 2002;54: 1153-1171.

[4] Noda H, Shimamoto T. Thermal pressurization and slip-weakening distance of a fault; an example of the Hanaore Fault, southwest Japan. Bull Seismo Soc America 2005;95:1224-1233.

[5] Wibberley C, Shimamoto T. Earthquake slip weakening and asperities explained by thermal pressurization. Nature 2005;436:7051:689-692.

[6] Wu YS, Pruess K, Persoff P. Gas flow in porous media with Klinkenberg's effect. Transport in Porous Media 1998;32:117-137.

[7] Faulkner DR, Rutter EH. Comparisons of water and argon permeability in natural clay-bearing fault gouge under high pressure at 20 degrees C. J. Geophysical Research 2000;105:16415-16426.

[8] Klinkenberg LJ. The permeability of porous media to liquids and gases. American Petroleum Institute, Drilling and Productions Practices 1941;200-213.

510 [9] Brace WF, Walsh JB, Frangos WT. Permeability of granite under high pressure.
511 Journal of Geophysical Research 1968;73:2225-2236.
512 [10] Zhang M, Takeda M, Esaki T, Takahashi M, Endo H. Effects of confining pressure
513 on gas and water permeabilities of rocks. Mat Res Soc Symp Proc 2001; 663.
514 [11] Furbish DJ. Fluid physics in geology; an introduction to fluid motions on earth's
515 surface and within its crust. New York: Oxford University Press, 1997.
516 [12] Zoback DM, Byerlee DJ. The effect of microcrack dilatancy on the permeability of
517 westerly granite. Journal of Geophysical Research 1975;80:752-755.
518 [13] Jones SC. A rapid accurate unsteady-state Klinkenberg permeameter. SPE Journal
519 1972;383-397.
520 [14] Persoff P, Hulen JB. Hydrologic characterization of reservoir metagraywacke from
521 shallow and deep levels of the geysers vapor-dominated geothermal system.
522 California, USA. Geothermics 2001;30:169-192.
523 [15] Teng LS. Geotectonic evolution of late Cenozoic arc-continent collision in Taiwan.
524 Tectonophysics 1990;183:57-76.
525 [16] Suppe J, Wittke JH. Abnormal pore-fluid pressures in relation to stratigraphy and
526 structure in the active fold-and-thrust belt of northwestern Taiwan. Petroleum
527 Geology of Taiwan 1977;14:11-24.
528 [17] Scheidegger AE. The physics of flow through porous media, 3rd Edition. Toronto:

529 University of Toronto Press, 1974.
530 [18] Chemical Society of Japan, Kagaku-Binran Kiso-Hen, 5th edition. Tokyo: Maruzen,
531 2004.
532 [19] Heid JG, McMahon JJ, Nielson RF, Yuster ST. Study of the permeability of rocks
533 to homogeneous fluids. API Drilling Prod Pract 1950;230-244.
534 [20] Jones FO, Owens WW. A laboratory study of low-permeability gas sands. J Petrol
535 Technol 1980;1631-1640.
536 [21] Sasaki T, Watanabe K, Lin W, Hosoya S. A study on hydraulic conductivity for
537 Neogene sedimentary rocks under low hydraulic gradient condition.
538 Shigen-to-Sozai 2003;119:587-592.
539 [22] Byerlee J. Friction, overpressure and fault normal compression. Geophys Res Lett
540 1990;17:2109-2112.
541 [23] Massey B, Smith JW. Mechanics of fluid, 8th edition. London and New York: Spon
542 press, 2005.
543 [24] Lever A, Dawe RA. Clay migration and entrapment in synthetic porous media.
544 Marine and Petroleum Geology 1987;4:112-118.
545 [25] Lever A, Dawe RA. Water sensitivity and migration of fines in the Hopeman
546 Sandstone. J Petroleum Geology 1984;7:1:97-108.
547 [26] Wu YS. Numerical simulation of single-phase and multiphase non-Darcy flow in

548 porous and fractured reservoirs. Transport in Porous Media. 2002;49:209-240.

Specimen symbol	Formation	Maximum burial depth (m)	Age (Ma)	Sample length (mm)	Sample diameter (mm)	Porosity (%)		Average pore radius (μm)
						Standard method	Mercury injection	
IVA407	Tungkeng Fm	3900-4500	11.6-14.5	20.8	20.6	22.7	18.8	4.75
IVA418	Shihmentsum Fm	4500-4800	17.8-19	12.4	20.7	13.6	11.9	0.76
IVA419	Kuanyinshan Ss	4500-4800	14-15	23.4	20.3	20.6	16.1	1.48
IVA478	Hourdonqkeng Fm	3900-4500	13.9-18	18.4	20.7	8.5	8.4	0.24

Modal pore radius (μm)
12.59
2.51
7.94
0.50

549 **Table caption**

550

551 **Table. 1 Information on specimens**

552

553

554 **Figure captions**

555

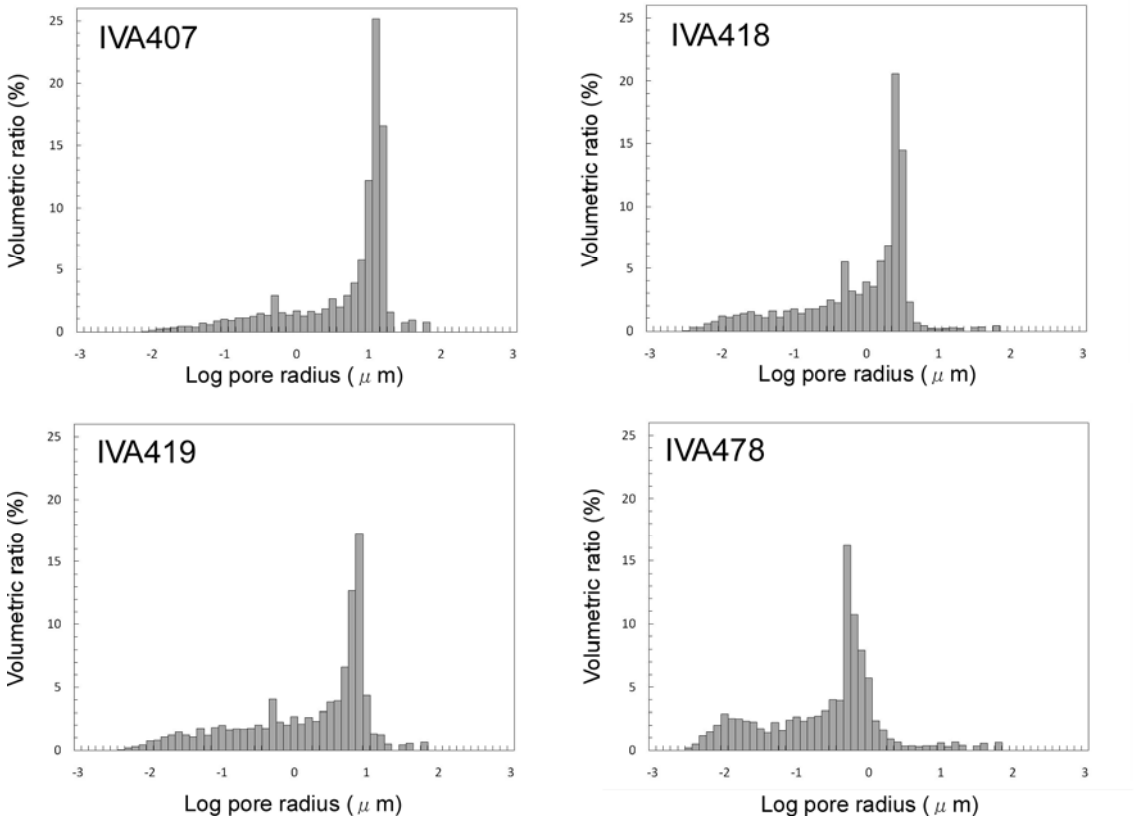

556

557 Figure 1. Pore-size distributions of the test samples.

558

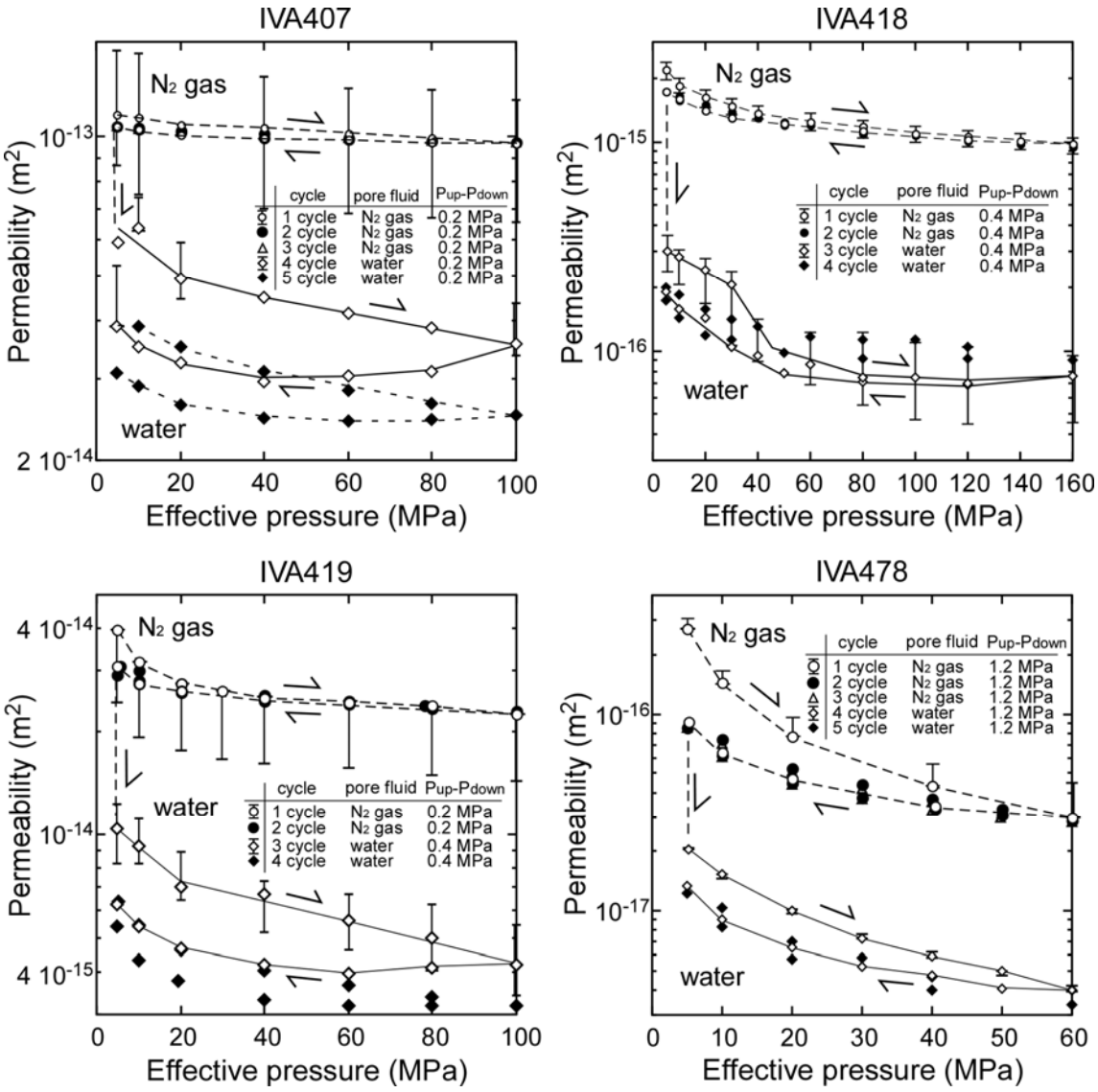

559

560 Figure 2. Relationship between permeability and effective pressure from the pressure

561 cycling tests. Nitrogen gas was used as the pore fluid in the first two or three pressure

562 cycles, and then distilled water was used in the last two pressure cycles. Error bars

563 mainly reflect the pore-pressure dependence of permeability.

564

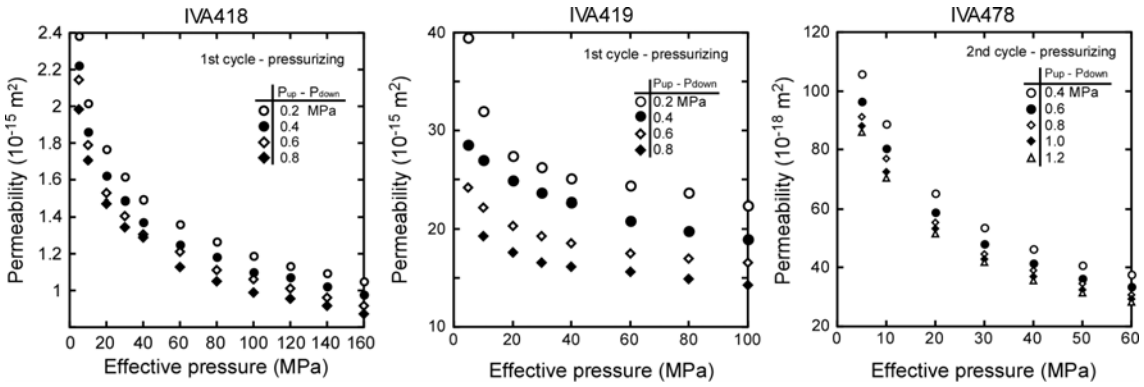

565

566 Figure 3. The dependence of permeability of a medium to nitrogen gas on the

567 pore-pressure differential.

568

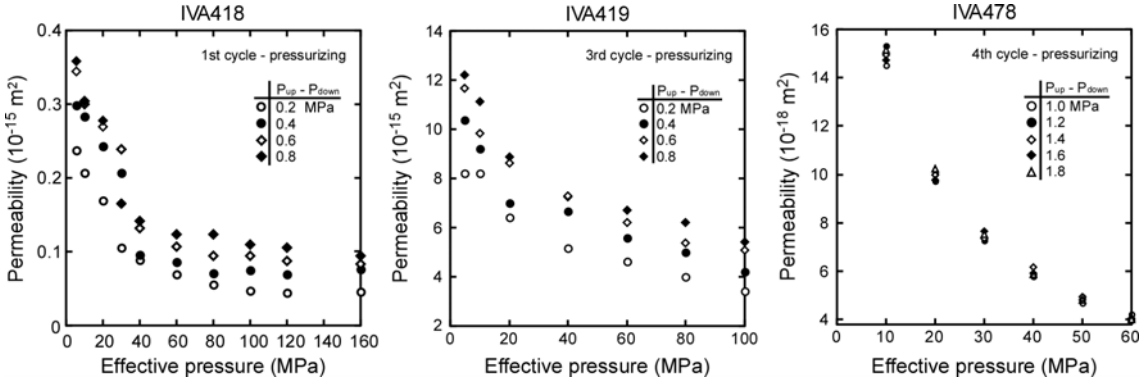

569

570 Figure 4. The dependence of permeability of a medium to water on the pore-pressure

571 differential.

572

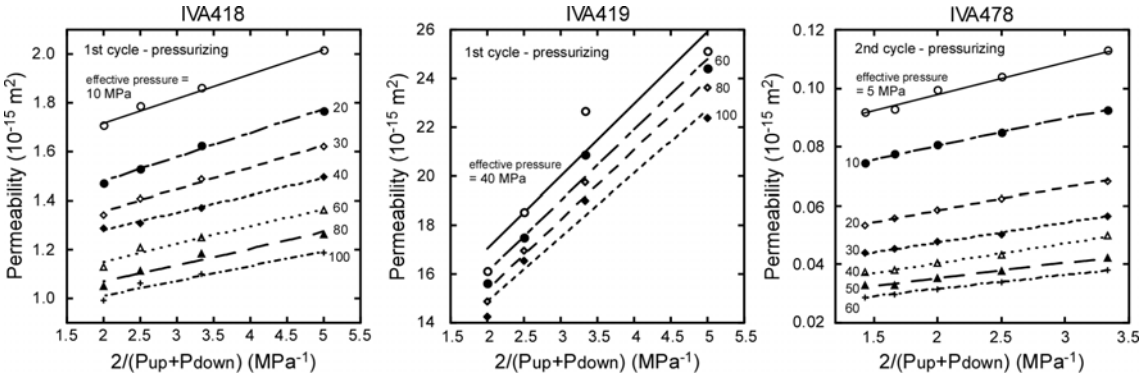

573

574 Figure 5. Relationship between permeability of a medium to gas and the inverse of the
575 average pore pressure, verifying the existence of the Klinkenberg effect described by
576 equation (2).

577

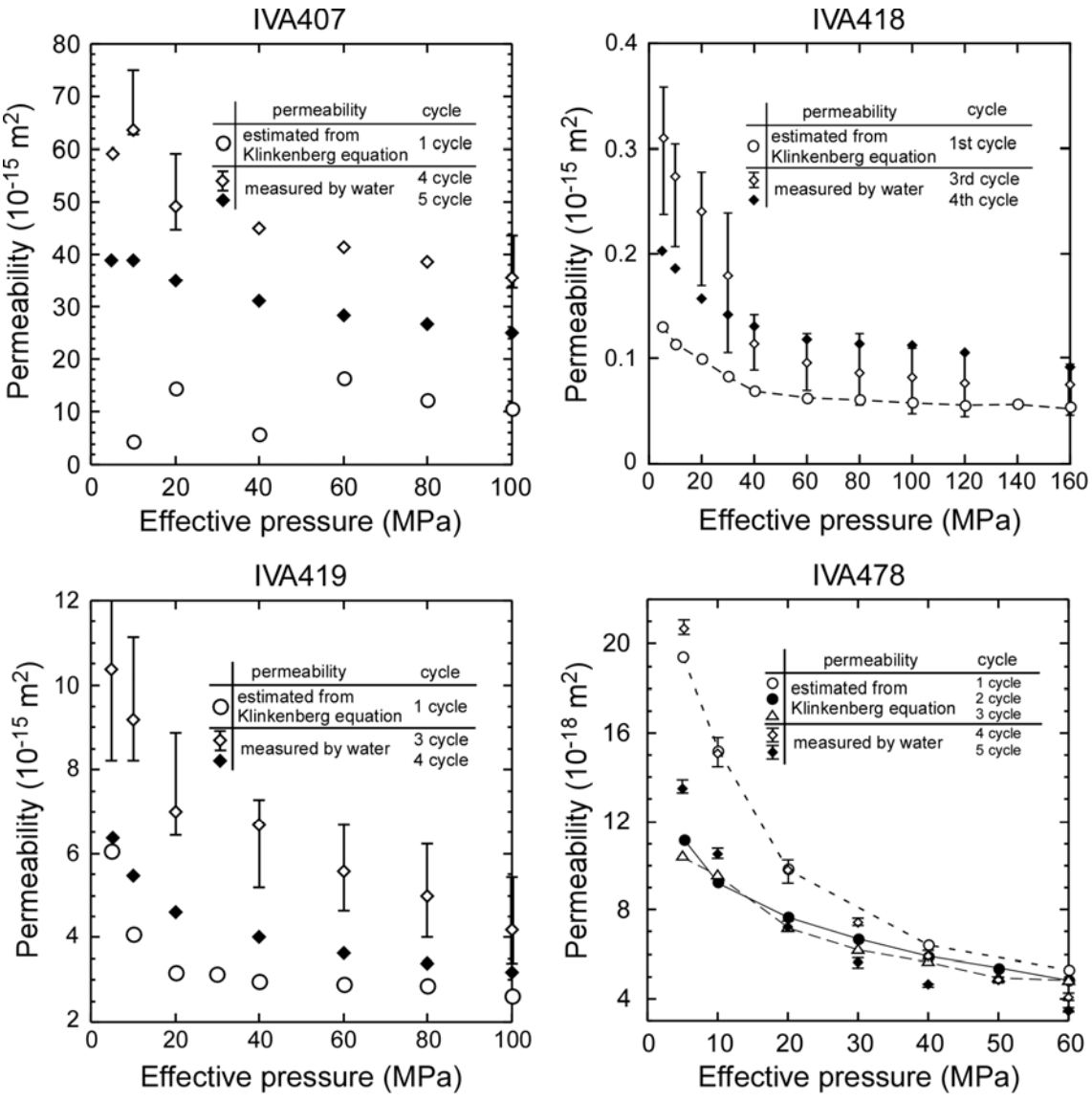

578

579 Figure 6. Comparison of water permeability estimated by using the Klinkenberg
580 equation and experimental data.

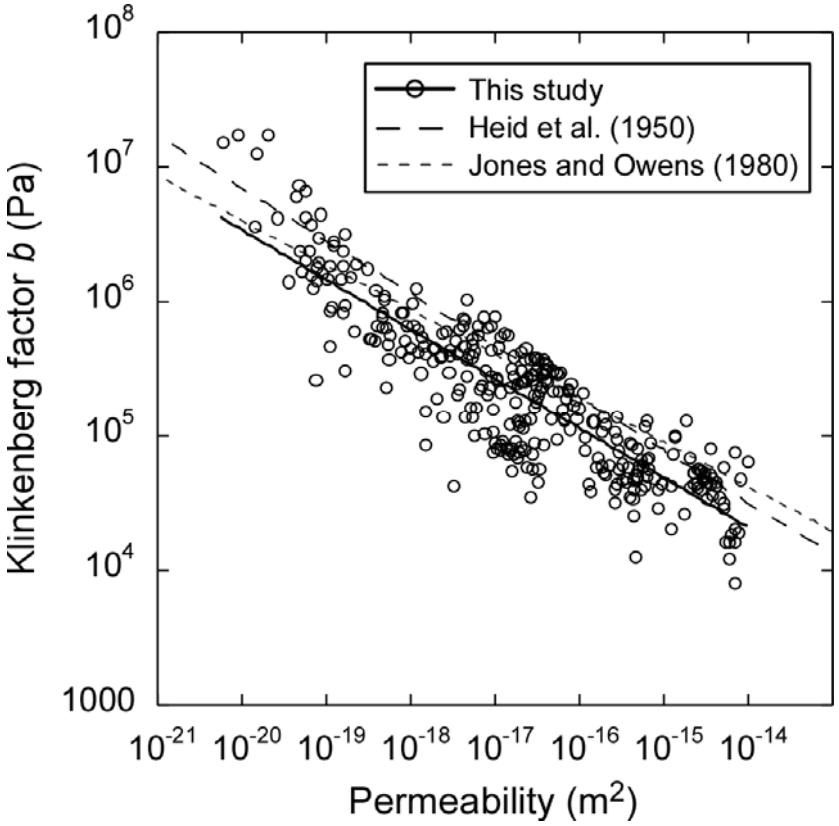

Figure 7. The Klinkenberg slip factor *b* and estimated water permeability power law relationship, obtained from the results of gas permeability tests of 30 sedimentary rocks from the Taiwan western foothills. The experimental data obtained by this study are compared with data from previous studies.

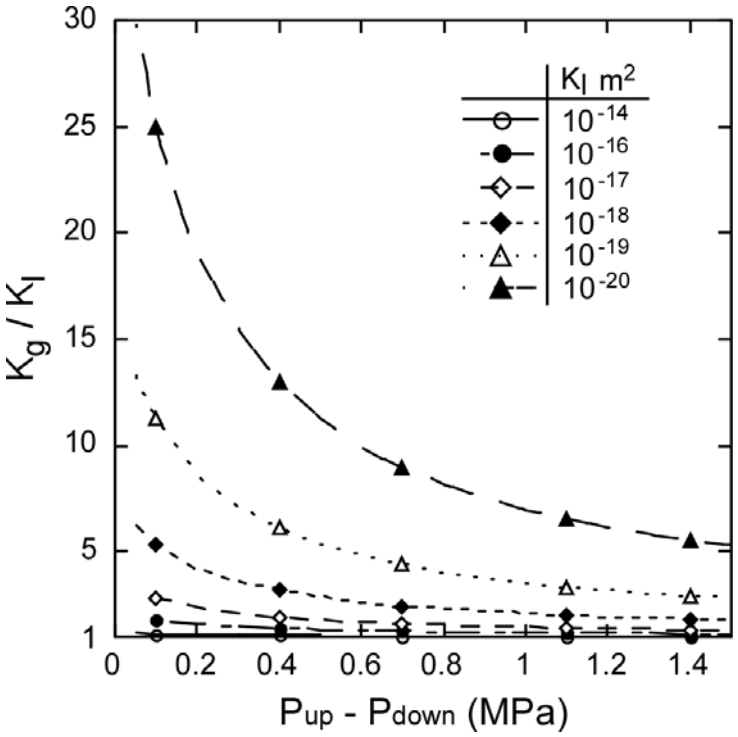

588

589 Figure 8. The relationship between the ratio of permeability of a medium to gas to that

590 to water and the pore-pressure differential, evaluated by using the empirical relationship

591 described by equation (8).

592

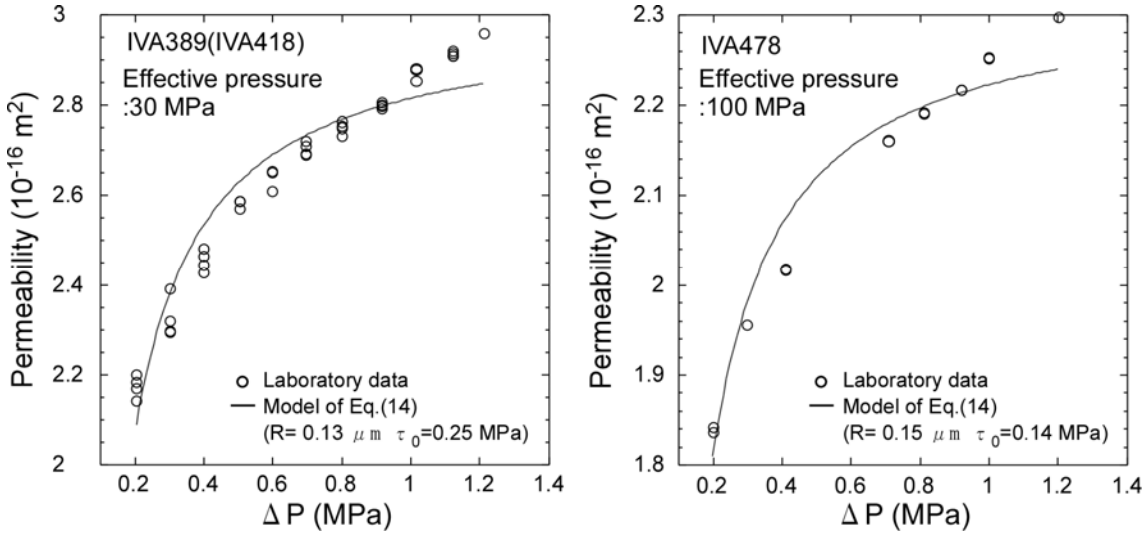

593

594 Figure 9. Dependence of water permeability on the pore-pressure differential. The

595 trends obtained in two specimens are compared to those predicted by the
596 Buckingham-Reiner model (equation 14), which is based on Bingham plastic flow into
597 an assembly of capillary tubes of the same pore radius.

598

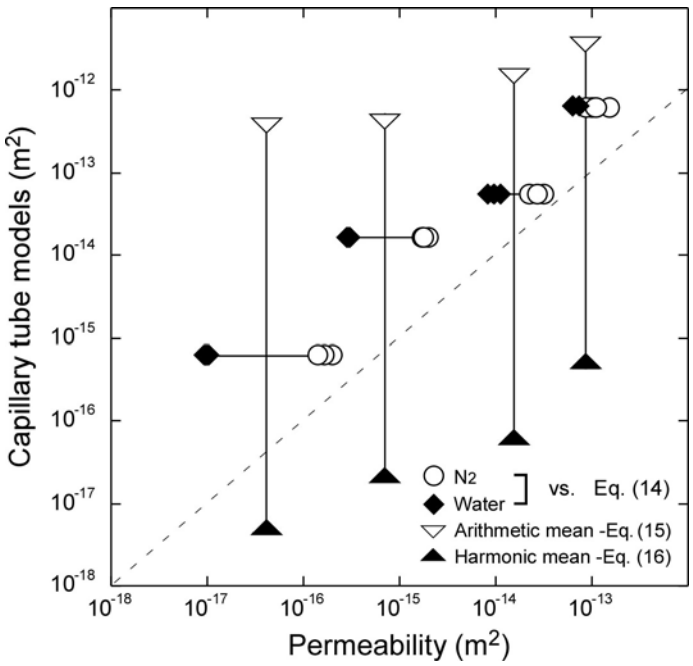

599

600 Figure 10. Comparison of observed permeabilities and the theoretical models of
601 equations (14), (15), and (16).